HHS Public Access

Author manuscript

Dev Cell. Author manuscript; available in PMC 2016 March 23.

Published in final edited form as:

Dev Cell. 2015 March 23; 32(6): 731–742. doi:10.1016/j.devcel.2015.01.027.

Light regulates the ciliary protein transport and outer segment disc renewal of mammalian photoreceptors

Ya-Chu Hsu[*,#], **Jen-Zen Chuang**[*,#], and **Ching-Hwa Sung**[*,+,@]

[*]Dyson Vision Research Institute, Department of Ophthalmology, Weill Medical College of Cornell University, New York, NY 10065

[+]Department of Cell and Developmental Biology, Weill Medical College of Cornell University, New York, NY 10065

Abstract

The outer segment (OS) of the rod photoreceptor is a light-sensing cilium containing ~1,000 membrane-bound discs. Each day, discs constituting the distal tenth of the OS are shed, while nascent discs are formed at the base of the OS through the incorporation of molecules transported from the inner segment. The mechanisms regulating these processes remain elusive. Here we show that rhodopsin preferentially enters the OS in the dark. Photoexcitation of post-Golgi rhodopsins retains them in the inner segment. Disc-rim protein peripherin2/rds enters the OS following a rhythm complementary to that of rhodopsin. Light-dark cycle-regulated protein trafficking serves as a mechanism to segregate rhodopsin-rich and peripherin2/rds-rich discs into alternating stacks, which are flanked by characteristic cytoplasmic pockets. This periodic cytostructure divides the OS into ~10 fractions, each containing discs synthesized in a single day. This mechanism may explain how the rod photoreceptor balances the quantity of discs added and removed daily.

Introduction

Vertebrate rod photoreceptors use a cylinder-shaped modified cilium, the outer segment (OS), as a light sensing organelle. Each OS contains ~1,000 orderly stacked disc membranes, creating a large surface area on which to display a high concentration of the photopigment, rhodopsin. Rhodopsin is synthesized in a region of the cell body called the inner segment (IS), and is transported to the OS through a narrow ciliary transition zone (i.e., connecting cilium) (Rohlich, 1975) (Fig. 1A). Mice lacking rhodopsin fail to form an

[@]Correspondence to: Ching-Hwa Sung, chsung@med.cornell.edu, Tel: 212-746-2291.
[#]Equal contribution

Authors' contributions: Y.-C. H., J.-Z. C., and C.-H. Sung conceived, designed, and carried out in vivo retina transfection experiments. Y.-C. H. and J.-Z. C. generated all constructs and carried out phenotypic analyses of transfected retinas. Y.-C. H. conducted immunoEM, DeepSeq, rod isolation, light condition experiments. J.-Z., C. conducted and analyzed TEM and FIM-SEM analyses. C.-H. S. provided funding. Y.-C. H., J.-Z., C., and C.-H. S. wrote the manuscript.

OS, a finding which suggests that, in addition to perceiving light, rhodopsin also plays a structural role in the genesis of the OS (Humphries et al., 1997; Lem et al., 1999).

Almost 50 years ago, Richard Young (Young, 1967; Young, 1968) showed that OS discs undergo constant renewal. Using in situ autoradiography Young found that pulse-labeled radioactive amino acids first appeared in the IS and then in the OS. The radioactive "reaction bands" formed at the base of the OS are displaced progressively toward the retinal pigment epithelium (RPE) immediately adjacent to the apex of the OS (LaVail, 1983; Young, 1967). The distalmost OS discs are shed in stacks and removed by RPE cells through phagocytosis (Bok and Hall, 1971; LaVail, 1983; Young, 1967, 1971). Using this method, Young elegantly showed that OS proteins live for ∼10 days before being degraded by RPE cells in rodents.

However, many key questions pertinent to OS disc renewal are difficult to address by autoradiography due to its low sensitivity, limited spatial resolution, and lack of protein tagging specificity. Further, no in vitro model system is available for the study of disc renewal. To date, the molecular mechanism that balances the number of disc membranes added and removed daily, and, hence, maintains a constant OS length, remain unclear.

In addition to rhodopsin, a cysteine-rich tetraspanin protein, peripherin2/rds (PRPH2) is also indispensable for the development of the OS (Cohen, 1983; Sanyal and Jansen, 1981; Travis et al., 1989). Unlike rhodopsin, which is primarily expressed on the lamellae of disc membranes, PRPH2 is specifically expressed along the rims of disc membranes and incisures (Kedzierski et al., 1996; Loewen et al., 2003; Molday et al., 1987; Tam et al., 2004). The shape of the OS disc membrane is not a perfect circle; disc incisures are cleavages generated by the infolding of the disc rim towards the center of the disc lamella. Transgenic frog studies showed that PRPH2 is functionally involved in the organization of disc incisures (Loewen et al., 2003; Tam et al., 2004). However, since the structure of disc incisures (i.e., number, depth, shape, location) varies greatly between amphibians and mammals (Cohen, 1960; Papermaster et al., 1978; Pedler and Tilly, 1967), the physiological importance of PRPH2 in the mammalian rod OS remains to be investigated.

Human mutations of both rhodopsin and PRPH2 are associated with a retinal degenerative disease called retinitis pigmentosa (RP) (Hartong et al., 2006), a leading cause of blindness and also a ciliopathy. Impaired rhodopsin localization and OS morphogenesis are common phenotypes associated with RP (Sung and Chuang, 2010). This underscores the importance of better understanding the mechanism that regulates OS protein transport and its interrelated processes of disc formation and renewal in photoreceptors. Here, we describe a novel approach for tracking the path and fate of newly synthesized rhodopsin and PRPH2 in rat rods. We found that light plays an instrumental role in regulating OS protein transport and cytostructure.

Results

Inducible expression system reveals the transport of newly synthesized rhodopsin in mammalian rods

To track newly synthesized rhodopsin without the interference of the highly abundant rhodopsin present on the OS, we employed a Cre-lox system to induce the expression of rhodopsin reporters in transfected rodent rods. Plasmids encoding ER^{T2}-Cre-ER^{T2} (under the CAG promoter) and rhodopsin reporter (under the CAG promoter followed by a loxP-neo-STOP-loxP cassette) were co-transfected into neonatal rat rods (Fig.1B). When the animals' retinas reached maturity (∼3 weeks old), a single dose of 4-hydroxytamoxifen (4OH) was administered to activate Cre and, hence, induce rhodopsin reporter gene expression by removing the neo-loxP cassette and the transcription stop signal. We refer to this inducible expression system as iP_{CAG} to distinguish it from the constitutive CAG expression system denoted by P_{CAG}.

In order to eliminate concerns surrounding epitope tagging and/or detection methods, we used several rhodopsin reporters, including untagged human rhodopsin (hRho), fluorescent protein-tagged rhodopsin (i.e., GFP, HcRed, mCherry), and small epitope-tagged rhodopsin (i.e., Flag, vsvg). Florescent and small epitope tags were added at the C-terminus and N-terminus of rhodopsin, respectively. For the former, the terminal 8 amino acids of rhodopsin were added back to the 3′-end of the tag to ensure the OS targeting (Fig.1 E; (Jin et al., 2003; Sung et al., 1994; Yeh et al., 2006). The distribution of hRho can be detected by a monoclonal antibody (mAb) 3A6, which specifically recognizes human, but not mouse, rhodopsin (MacKenzie et al., 1984). When hRho was used, rods were subjected to a 1-hr dark adaptation period prior to harvest in order to unmask the epitope (Chuang et al., 2004). Rods transfected with fluorescent protein-tagged rhodopsin were directly detected by their emitted fluorescence.

As predicted (Fig.1C), after 24-hr 4OH induction, both hRho (Fig.1D) and Rho-GFP (Fig. 1F) appeared as single compact bands at the most proximal OS region (i.e., nascent discs). In these experiments, photoreceptor cadherin was used to mark the base of the OS plasma membrane (Rattner et al., 2001).

To reveal the distribution of newly synthesized rhodopsins before they reach OS, we examined rods expressing Rho-GFP (Figs.S1A, S1B) and hRho (Fig.S1C) for 12 hr. To our surprise, only a subset of nascent rhodopsins had overlapping distribution with the TGN38-labeled trans-Golgi network, which was restricted to the basal part of the IS (Fig.S1B); the majority of the rhodopsin was found throughout the IS and in the synapse (Figs.S1A, S1B). The rhodopsin signals in the IS were frequently found on compartments (∼0.3-0.5 μm in diameter) likely representing recycling endosomes, as they expressed Rab11a (or Rab11a-GFP) and transferrin receptor (Figs.S1C, S1D). Furthermore, immunoEM demonstrated co-distribution of endogenous rhodopsin and Rab11a in the IS (Fig. S1E). These results suggest that rhodopsin transits through an intermediate compartment prior to reaching the OS.

Rhodopsin enters the OS in a diurnal rhythm

As anticipated, the signals of rhodopsin reporters extended distally from the base of the OS as time progressed following 4OH induction. Of great interest, all rhodopsin reporters tested — hRho (Fig.2A), Rho-HcRed (Fig.2B), Rho-GFP (data not shown), and vsvg-Rho (data not shown) — displayed banding patterns with alternating strong and weak signals in the OS. Interestingly, the number of strong bands correlated closely with the number of days after 4OH induction (Figs.2A, 2B). The P_{CAG}-directed rhodopsin reporters — FLAG-Rho (Fig.2C; detected by FLAG immunoreactivity) and Rho-mCherry (Fig. 2D) —also displayed similar banding patterns when constitutively expressed in rods. Thus, these results also indicate that neither the type of epitopes nor the position of the tagging affects the OS trafficking of rhodopsin reporters.

We then showed that hRho driven by the promoters for the opsin gene (or P_{opsin}; Fig.2E) and Nrl gene (or $P_{NRL;}$ data not shown) also displayed similar banding patterns, indicating that the oscillating expression pattern of rhodopsin is unlikely to be a consequence of promoter-specific transcriptional regulation.

We also performed qRT-PCR of RNAs isolated from the FACS-sorted, transfected rods expressing P_{CAG} -Rho-GFP, and showed that the exogenous rhodopsin only contributed ∼2% of total rhodopsin (Fig.S2A). Furthermore, using a (pan)anti-rhodopsin Ab that recognizes both endogenous (rat) rhodopsin and exogeneious (human) rhodopsin reporter, we showed that the total rhodopsin level was indistinguishable between transfected and non-transfected rods (Fig.S2B). These results suggest that the banding pattern of rhodopsin reporter is unlikely caused by transgene overexpression.

Exposure to light inhibits the delivery of rhodopsin to the OS

The above results suggest that rhodopsin enters the OS according to a diurnal rhythm. To distinguish whether the periodicity of rhodopsin's entry into the OS is driven by circadian rhythm or exposure to light, we examined rats subjected to a series of light regimens. Rats constitutively expressing hRho reared in regular cyclic light (12hr light:12hr dark) for 3 weeks and moved to constant dark for 4 days before harvest no longer exhibited the banding pattern at the proximal OS region (Figs.3A, 3B). Reproducible results were obtained when P_{CAG} (Fig.3A) and P_{opsin} (Fig.3B) promoters were used. Furthermore, hRho induced to express for 4 days in the dark was homogeneously expressed in the basal OS without obvious bands (Fig. 3C). These results, taken together, suggest that the delivery of rhodopsin into the OS is regulated by light rather than circadian rhythm.

The above results also imply that darkness represents a permissive condition for targeting rhodopsin to the OS. Supporting this, almost all transfected iP_{CAG}-Rho-GFP was detected in the OS of the rats kept in complete darkness during 2-day induction (Fig.3D, left). In contrast, Rho-GFP was predominantly retained in the cell body when animals were kept in constant ambient light during the 2-day induction (Fig.3D, right). Furthermore, normal (untransfected) mouse (Fig.S3A) or rat (data not shown) rods experienced prolonged light exposure (e.g., 4-day constant light) had detectably more rhodopsins expressed in the cell bodies compared to their counterparts kept in regular cyclic light.

We then asked whether a dark adaptation is sufficient to remove the light-mediated accumulation of rhodopsin in the cell body. To this end, we compared animals that had rhodopsin induced for 1 day in regular cyclic light and then harvested at noon with or without 1-hr dark adaptation. The animals receiving dark adaptation had the large majority of Rho-GFP rhodopsin in the OS, whereas those that were not dark adapted had a significant amount of Rho-GFP retained in the IS (Fig.3E).

Finally, we tested how the distribution pattern of the rhodopsin reporter varies in animals harvested at different times of the day. In these experiments, rats were induced to express Rho-GFP for 2 days in cyclic light, and then harvested at either 6 pm (before the lights were switched off) or 7 pm (1 hr after the lights were switched off). The large majority (~72.9%) of rods harvested at 6 pm had Rho-GFP signal in the cell bodies (Fig.3F, left). In sharp contrast, most rods (~70.5%) harvested at 7 pm had Rho-GFP signals confined to the base of the OS (Fig.3F, right). These results collectively argue that light exposure inhibits the entry of rhodopsin to the OS; a brief dark adaptation can effectively reverse this process.

Rhodopsin in the rod IS can be photoexcited

The above findings indicated that newly synthesized rhodopsin in the IS is able to sense light. We thus predict that the IS-localized rhodopsin may also undergo its light-triggered conformational change and bind to visual arrestin (v-arr) just as it does in the OS (Baylor, 1996). Supporting this idea, we first showed that endogenous v-arr and rhodopsin were colocalized in the IS of light-adapted rods by immunoEM (Fig. S3B). Furthermore, we predicted that RP mutants with a conformation mimicking constitutively photoexcited rhodopsin (e.g., R135L, K296E; (Chuang et al., 2004; Robinson et al., 1992; Shi et al., 1998) would have difficulty entering the OS even in the dark. Indeed, we observed that both the iP_{CAG}-directed R135L-GFP (Fig.3G) and K296E-GFP (data not shown) were largely retained in the rod IS/cell body/synapse of rats reared in constant darkness during the entire 2-day induction period.

Subsequently, we used the ability to bind v-arr as a readout for the conformational state of the rhodopsin in the biosynthetic pathway. Here we employed the RP mutant rhodopsin Q344ter (lacking the C-terminal 5 residues that contain the OS targeting VxPx signal; (Sung et al., 1994) as a reporter for the rhodopsin retained in the biosynthetic pathway. Q344ter has a normal ability to sense light and bind v-arr (Sung et al., 1994). In normal light-adapted rods, v-arr is predominantly localized in the OS, due to its high-affinity interaction with photoexcited rhodopsin, whereas in normal dark-adapted rods, v-arr is predominantly localized in the rest of rod cell bodies (Arshavsky, 2003; Whelan and McGinnis, 1988). Like the endogenous v-arr, singly transfected GFP-v-arr also followed the light triggered OS translocation (Fig.3H). However, in light-adapted rods that also co-expressing Q344ter, there was a prominent increase in GFP-v-arr colocalized with the Q344ter in the IS/cell body/synapse (Fig.3I).

Finally, we reasoned that GFP-v-arr should also be able to reveal the distribution of endogenous rhodopsin in the OS due to their high affinity interaction stimulated by light. We showed that constitutively expressed GFP-v-arr (Fig.S3C) and FLAG-v-arr^{p44} (Fig.S3D) exhibited a banding pattern in the transfected OS. V-arr^{p44} is a naturally

occurring truncated splicing variant that also binds to photoactivated rhodopsin, just like normal v-arr (Moaven et al., 2013). In our hands, FLAG-v-arr^{p44} did not formed aggregates in transfected rods as GFP-v-arr occasionally did. FLAG-v-arr^{p44} was then used to test whether prolonged dark exposure would alter the OS distribution of endogenous rhodopsin, as predicted by our model. In these experiments, iP$_{CAG}$-Flag-v-arr^{P44} and iP$_{CAG}$-vsvg-Rho were co-transfected in neonatal rat rods, and at the age of PN21, these rats were either still maintained in regular dark-light cycle or transferred to complete darkness for 9 days. The rat eyes were then harvested under light one day after 4OH induction. In both cases, the vsvg-Rho expressed for one day was confined to the OS base, but FLAG-v-arr^{P44} was able to diffuse throughout the entire OS (Fig.S3E, S3F). While FLAG-v-arr^{P44} was expressed in bands in rats reared in cyclic light (Fig.S3E), this periodic pattern was largely abolished in the rats reared in constant dark (Fig.S3F). These results support the idea that the OS entry of endogenous rhodopsin also follows a light-regulated pathway, and rhodopsin preferentially enters the OS in the dark.

Discs synthesized during the day and night are heterogeneous in protein composition

To test whether another disc membrane protein also exhibits an oscillating expression pattern in the OS, we examined the disc rim protein PRPH2. In rods expressing iP$_{CAG}$-driven PRPH2-GFP for one day, fluorescence was largely confined to the base of the OS (Fig.4A, left panel). PRPH2-GFP signals also oscillated along the OS axis in rats reared in cyclic light and harvested at a later time point (i.e., 4 days) (Fig. 4A, right panel). The number of bands containing bright PRPH2-GFP signal also correlated with the number of days of induction. The expression of PRPH2-GFP driven by the constitutive P$_{CAG}$ promoter appeared as ∼10 bands along the axis of the OS (Fig.4B, left panel).

Most interestingly, when rods co-expressed PRPH2-GFP and hRho, their respective signals appeared to alternate; the regions displaying stronger hRho signals exhibited weaker PRPH2-GFP, and vice versa (Fig.4C, Movie 1). Since both rhodopsin and PRPH2 reporters were expressed under the same P$_{CAG}$ promoter, their complementary oscillating expression patterns are unlikely to be caused by regulation at the transcriptional level.

A thin PRPH2-GFP-labeled “line” running parallel to the OS axoneme (open arrows, Figs. 4B right panel, 4C) likely represented the composite signals of PRHP2 expressed on the incisures of all discs that registered in alignment along the axis of the OS (also see Fig.6).

Endogenous rhodopsin and PRPH2 exhibit a complementary periodic pattern

If the ectopically expressed reporters faithfully recapitulate what happens endogenously, why has this banding pattern of rhodopsin and PRPH2 not been observed in the past using standard immunostaining protocols? First, previous immunoEM studies of these two molecules have been primarily qualitative, or have focused on partial areas of the OS or isolated discs (Arikawa et al., 1992; De Robertis, 1960; Fekete and Barnstable, 1983; Hicks and Molday, 1986; Jan and Revel, 1974; Molday et al., 1987; Nir and Papermaster, 1983; Travis et al., 1991). Second, the distribution pattern of rhodopsin (i.e., plasma vs. disc membranes) can be greatly influenced by the epitope recognition sites of the Abs used for detection (Hicks and Molday, 1986). Third, localization studies using light microscopy have

been primarily conducted under low magnification. In our experiments, endogenous rhodopsin labeling appeared to be homogeneously bright across the entire OS layer under the low-power examination (Fig.S4A). Upon high-power examination we found that the Ab recognizing rhodopsin's N-terminus (facing the extracellular side) predominantly labeled the OS plasma membranes rather than the disc membranes inside the OS (Fig.S4B), even though the latter is the site that houses the majority of the rhodopsin molecules. Intriguingly, the few rods which had rhodopsin labeling inside the OS exhibited the banding pattern (Fig.S4C, arrow). This observation indicates that rhodopsin on the disc membranes are far less accessible to the Ab relative to the rhodopsin residing on the plasma membrane.

To increase our chance of visualizing the rhodopsins that localize on the discs, we briefly treated retinal slices with neuraminidase, then labeled them with Abs that bind to rhodopsin's cytoplasmic C-terminus. We used 40-μm-thick vibratome sections (instead of ∼8-μm frozen sections) to be able to better label the entire OS which is ∼17-30 μm long (LaVail, 1973), and is not always parallel to the sectioning plane. Using these techniques, we found that the immunolabeling of endogenous rhodopsin and PRPH2 also exhibited an alternating distribution pattern along the axis of the rod OS (Fig.4D). Each OS appeared as though it were divided into ∼7-12 segments. Intense rhodopsin labeling was found within the bands themselves, whereas PRPH2 labeling showed up as “ring-like” shapes flanking the rhodopsin-rich disc segments (Fig.4D). The characteristic pattern was consistently observed in both pigmented C57BL/6J mice (Fig.4D) and non-pigmented Sprague Dawley albino rats (data not shown). Subsequently, we performed quantitative analysis of immunoEM of rhodopsin and PRPH2. These studies showed that the number of rhodopsin- and PRPH2-immunogold particles fluctuated along the length of individual OS; 8-10 peak signals (with 1.5-2.2 μm intervals) spanning along an individual rod OS could be identified for both molecules (Fig.4E).

To complement the immunostaining carried out in retinal slices, we showed that the segmented and complementary expression patterns of rhodopsin and PRPH2 on the OS were also readily visible in isolated rods (Fig.4F, Fig. S4D). Finally, we performed DeepSeq analyses using retinal RNAs isolated from mice kept in cyclic light (12h:12h) and harvested every 4 hours at different times of the day. These results showed that the transcript level of both rhodopsin and PRPH2 remained fairly constant between day and night (Fig.S4E). This finding argues against the idea that the OS periodicity of rhodopsin and PRPH2 is the result of oscillating transcription.

Morphological characterization of the disc heterogeneity and OS cytostructure

The above results suggest that cyclic light triggers a mechanism that allows discs with different protein composition to be segregated into distinct segments that alternate along the OS. Previous characterization of individual isolated discs have revealed morphological heterogeneity (Pedler and Tilly, 1967), but the organization of these discs in the rod OS was unknown. We were intrigued by the possibility that discs with different protein compositions have distinct structures. Because the OS has an overall limited cytoplasmic space due to densely packed discs, we envisioned that the shape of the disc could be reflected by the

volumes of surrounding cytoplasmic space, which can be indicated by the transfected soluble GFP.

Transfected GFP was typically bright throughout the IS, but overall weak in the OS except a few bright spots (Fig 5A). Closer inspection of the OS co-expressing both GFP and h-Rho or PRPH2-mCherry revealed that the rhodopsin-rich discs contained little GFP signal (brackets, Fig.5B), whereas PRPH2-rich discs contained modest GFP signal (brackets, Fig. 5C). These results indicated that, compared to rhodopsin-rich discs, the PRPH2-rich discs were surrounded by a larger cytoplasmic space, likely due to their expanded rims and incisures. Interestingly, brightest GFP signals (or hotspots) were associated with neither the rhodopsin nor PRPH2-rich discs. Instead, they were specifically localized to the edges right between rhodopsin-rich and PRPH2-rich disc segments (open arrows, Fig.5B, 5C). These results imply that the discs synthesized during the phase transition between day and night are surrounded by most expanded cytoplasmic space; these discs are smaller and had low expression of both rhodopsin and PRPH2.

We subsequently showed that the GFP hotspot distribution pattern also altered following the change in light conditions. In these experiments, rats were first reared in cyclic light and then switched to constant dark for 4-5 days. While the typical GFP hotspots were found in the distal OS (arrows, Fig. S5), they were specifically absent in the proximal OS (bracket, Fig.S5). This phenomenon was consistently observed in rods either co-transfected with (Fig.S5) or without (not shown) h-Rho.

Three-dimensional composed confocal images showed that the GFP localized to the OS appeared like a beaded necklace coiled around the entire OS; two adjacent beads (hotspots) were often situated diagonally across the OS (Supplementary Movies 2, 3). Using high-power transmission EM (TEM), we were able to detect a prominent expanded cytoplasmic space periodically expressed along the OS axis (greens, Figs.6A-6B), herein we refer to this structure as Outer Segment Cytoplasmic Pocket (OSCP). The GFP hotspots of transfected rods likely represent the OSCP, both appeared intermittently along the OS axis and confined to one side of the OS (disc membrane).

To further characterize the OSCP and disc heterogeneity, we turned to the use of focused ion beam scanning electron microscopy (FIM-SEM), an ultrastructural analysis method that allows automated precision milling of tissue blocks and consecutive imaging of hard-fixed specimens. Indeed, the serial block-face images we obtained demonstrated superior membrane preservation of OS discs and structures. These studies showed that, in addition to the discs having a highly compact appearance, there were also disc stacks that had a porous, spongy appearance due to increased cytosol contacts; the spongy disc stacks were observed in a periodic pattern along the OS axis (brackets, Figs.6C, 6D; Supplementary Movie 4). Taken together the aforementioned GFP expression studies, we predicted that the compact discs and spongy discs represented rhodopsin-rich and PRPH2-rich discs, respectively. Finally, we were able to identify characteristic OSCP (black arrows, Figs 6C-6D; Supplementary Movie 4) and their associated small discs.

Toward the distal OS, both the spatial confinement and structures of the OSCP became increasingly irregular (green, Figs.7A-7C). At the distal end, where disc stacks prepare to be shed, they were often bent at the regions containing discs with prominently enlarged incisures as well as OSCPs (black and curved arrows; Fig.7C). Furthermore, the OS apices were frequently capped by an enlarged cytoplasmic space (Figs.7A-7C; S6A-6D).

Finally, both TEM and FIM-SEM showed that both electron dense materials and small vesicular profiles in OSCPs were readily detectable (Figs.6A-6D, S6A-6E, 7A-7B). In particular, structures characteristic for late endosome/multivesicular body (MVB) and/or autophagosome were frequently found in the distal OSCP (Figs.S6A-S6D, 7A, 7B). In supporting this, LAMP1, a marker for these two closely related degradation organelles, was frequently found on GFP hotspots (Fig.S6F). These observations collectively are consistent with the idea that the OSCP serves as a breaking point during OS disc shedding; the materials contained within might participate in the process preparing for these cellular processes.

Discussion

By applying the plasmid based Cre-lox mediated gene induction system, we were able to pulse express two disc membrane proteins in rat rods exposed to different lighting conditions. Unexpectedly, these studies show that OS disc membranes are heterogeneous in both protein composition and structure. However, these heterogeneous discs are arrayed in a specifically organized fashion. That is, rhodopsin- and PRPH2-rich discs are arrayed in alternating stacks, roughly dividing the OS into ∼10 fractions (Fig. 7D).

Several lines of independent evidence argue that these findings are not a phenotype caused by misexpression. (1) The expression level of rhodopsin reporters contributes only ∼2% of the total rhodopsins in the transfected rods. Besides, we only examined transfected rods that did not display apparent overexpression. (2) Non-tagged h-Rho, N-terminus tagged, and C-terminus tagged rhodopsins all share a similar banding pattern. Furthermore, the type and the location of the taggings (e.g., FLAG, vsvg, mCherry, GFP) made no difference in the expression pattern of the rhodopsin reporters. Similarly, the banding pattern was consistent between the non-tagged bovine PRPH2 (not shown), PRPH2-GFP, and PRPH2-mCherry.

Consistently, endogenous rhodopsin and PRPH2 immunolabeling (in both intact retina and isolated rods) and immunoEM assays suggested that these two proteins, and their transfected reporters, also had a complementary oscillating expression pattern in the OS. Finally, the expression pattern study of GFP-v-arr (a reporter for endogenous photoexcited rhodopsin) provides an additional independent line of evidence supporting the fluctuating expression of rhodopsin in the OS and the light-mediated regulation of its OS entry.

Light regulates the OS transport of rhodopsin

Our present findings are physiologically relevant and greatly further our understanding of OS disc renewal. First, our data show that the trafficking of rhodopsin from the IS to the OS oscillates during cyclic light, and is suppressed by light. As a result, nascent discs assembled during the night have a higher concentration of rhodopsin than those assembled during the

day. This result can explain why previous studies found that the OS of rats reared in constant dark are characterized by a significantly higher rhodopsin packing density (i.e., lower phospholipid: rhodopsin ratio) than those reared in cyclic light (Battelle and LaVail, 1978; Organisciak and Noell, 1977; Penn and Anderson, 1987; Williams et al., 1999).

Second, we found that post-Golgi rhodopsin transits through Rab11a+ recycling endosomes before entering the OS (Fig.7E). Light stimulation retains rhodopsin in these endosomes (and perhaps other intermediate compartments). These findings support the emerging theory that molecules traveling through the secretory pathway often stop at recycling endosomes before reaching their distal destination, a strategy that might be useful for further recruitment, (re)sorting and/or regulatory exocytosis (Thuenauer et al., 2014; Weisz and Rodriguez-Boulan, 2009). We are intrigued by the synaptic location of newly synthesized rhodopsin, this may explain why mislocalized rhodopsin was often found in the synapse of RP diseased rods.

Third, our current finding also argue that rhodopsins in the biosynthetic pathway have the ability to respond to light and bind to v-arr even before entering the OS. Conceivably, the “dark” rhodopsin can bind to the trafficking machinery that is required for its subsequent transport to the OS, whereas photoexcited rhodopsin cannot (Fig.7E). Previous studies showed that rhodopsin's binding site for v-arr partially overlaps with its OS targeting signal (Chuang et al., 2004; Raman et al., 2003). A brief dark adaptation can reverse the interaction between v-arr and photoexcited rhodopsin (Gurevich et al., 2011). Furthermore, removal of v-arr can largely rescue the IS mislocalization of photoactivated rhodopsin-mimicking K296E mutant (Chen et al., 2006). Therefore, it is tempting to speculate that v-arr may negatively regulate the OS entry of photoexcited rhodopsin, a model that awaits experimental test. Since all our studies were carried out in adult rodents, our finding is most relevant to the OS disc renewal in mature rods; the presence of a similar mechanism in developing rods remains unknown.

Oscillating OS protein transport pattern contributes to the disc heterogeneity and OS cytostructure

Fourth, our data show that PRPH2 enters the OS following a rhythm complementary to that of rhodopsin. As a result of the alternating OS entry of rhodopsin and PRPH2, discs synthesized during the day (rich in PRPH2) and night (rich in rhodopsin) have distinct protein compositions. Using soluble GFP to probe the cytoplasmic space, our observation suggested that these two types of discs also have different shapes and/or sizes. We envision that discs with abundant PRPH2 are likely to have expanded rims and, hence, more infoldings (and/or deeper incisures). This may account for their porous ultrastructural appearance. On the other hand, OS disc had higher level rhodopsin tend to have a larger lamellae and a smaller incisures (Wen et al., 2009). These findings, taken together, suggest that OS discs are structurally heterogeneous, a consequence caused by their different protein compositions.

Earlier detection of “birefringence bands” using polarized light microscopy has suggested that the structure of the disc membranes along the axis of the frog OS is not uniform (Corless and Kaplan, 1979). The periodic birefringence band pattern can also be disrupted

when the frogs are maintained in either constant dark or constant light (Kaplan, 1981). Rhodopsin and PRPH2 reporters transgenically expressed in frog OS are also displayed in bands, albeit less regular (Tam et al., 2000; Tam et al., 2004). Recently, Haeri (Haeri et al., 2013) showed that the rhodopsin-GFP in transgenic frog OS also exhibits a light-dependent periodicity. However, these authors concluded that this phenomenon was caused by the GFP tagging because they were unable to detect a similar banding pattern for endogenous rhodopsin. Since the morphology of the disc incisures (Tam et al., 2004) and the time required to renewal an OS (i.e., 4-8 weeks in frog; (Young, 1967) are very different between frogs and rodents, whether the birefringence bands seen in the frog OS are caused by the same mechanism we revealed in the rat OS remains to be resolved.

Our unpublished data showed that transfected ROM1 (a rim protein that binds to PRPH2; (Bascom et al., 1992; Goldberg and Molday, 1996) was co-enriched specifically with the discs that had high level of PRPH2, reiterating the targeting specificity of transfected protein in rods. Since the rim proteins do not sense light, the mechanism that governs their OS entry remains unknown. One hypothetical model is that PRPH2 can only enter the OS when rhodopsin's OS traffic is low, as rhodopsin outcompetes a common transport carrier, machinery, and/or route.

The rhythmatic patterning of rhodopsin and PRPH2 is unlikely to be a consequence of transcriptional regulation because (1) the rhodopsin reporters driven by several different promoters had a similar expression pattern, (2) the patterns of rhodopsin and PRPH2 driven by the same P_{CAG} promoter are not the same, instead, they were complementary, (3) the light-mediated OS entry inhibition of newly synthesized rhodopsin can be effectively reversed by a 1-hr dark adaptation, a time period far shorter than an average mRNA synthesis rate (3-5 h ; (Bolouri and Davidson, 2003), (4) the transcript levels of endogenous rhodopsin and PRPH2 did not fluctuate through the day, and didn't differ significantly in light vs. dark. Additionally, fluctuating disc synthesis rates cannot be held accountable for the OS periodicity of rhodopsin and PRPH2 because these two proteins, in fact, have a complementary expression pattern.

Finally, an even higher order of disc heterogeneity was revealed by our GFP mapping study. The discs synthesized during the day-night transition express low levels of both rhodopsin and PRPH2, and hence, are smaller. Stacking of these small discs yields an expansion of their surrounding cytoplasmic space (OSCP). Prolonged dark exposure depletes OSCP, implying that the light condition switch is required for the formation of the OSCP. Other factor(s) participating OSCP genesis remain to be investigated.

A cell autonomous mechanism maintains OS homeostasis

Our present study independently recapitulates Young's finding that OS proteins undergo constant renewal and have a life span of ∼10 days (Young, 1967). However, different from Young's pulse-labeling method, our method allows the iP_{CAG}-directed reporter to be constitutively expressed once it has been activated. These results reveal that rod cells pack one day's worth of rhodopsin-rich discs into a single “segment”, and each OS has total of ∼10 such segments. It is reasonable to hypothesize that the segmented arrangement of the

OS provides an autonomous structural cue for the rod to match the quanta of discs shed and added daily (Fig.7D). By this mechanism, the length of OS can be maintained in constancy.

In the above model, we propose that PRPH2-rich discs serve as pre-marked breaking points for disc shedding. By forming disulfide-linked oligomers under oxidizing conditions, PRPH2 alone is sufficient to initiate membrane hairpin structures (Wrigley et al., 2000). Furthermore, PRPH2 has a fusogenic activity (Ritter et al., 2004). It is therefore plausible that the distalmost PRPH2-rich discs are rather susceptible to structural damage due to accumulated oxidative stress. Additionally, the direct interaction between PRPH2 and OS plasma membrane molecules Na/Ca-K exchanger and cGMP-gated channel (Poetsch et al., 2001) may offer a putative physical tether to completely snap off a packet of discs from its tip, an area devoid of an axoneme (Insinna and Besharse, 2008). On the other hand, the OSCP in the distal OS might be involved in partial degradation of the discs in preparation for disc shedding. The OSCP may also provide a central hub for dynamic molecular exchange and vesicular trafficking (e.g., fission of shedded discs).

If our model is correct, mice hypomorphic for PRPH2 should be less effective in the placement of pre-assigned breaking points. Supporting this, PRPH2 has been implicated in OS disc shedding; the number of discs within nascent phagosomes of RPE cells is significantly higher in PRPH2 (rds/+) heterozygotes than in wild type mice (Hawkins et al., 1985). Our model also predicts that mice reared in constant dark would be expected to have fewer PRPH2-rich discs and OSCP to generate the breaking points for disc removal. Indeed, rats reared in constant dark have much longer OS than those reared in cyclic light (Battelle and LaVail, 1978; Penn and Williams, 1986). Future studies are warranted to more directly test our model, as well as to further delineate the molecular machinery, microenvironmental niche, and the contribution of RPE to distal OS disc removal.

Experimental Procedures

In vivo retinal transfection

All methods that involved live animals were approved by the Weill Medical College of Cornell University Institutional Animal Care and Use Committee. DNA (2-3 μg total) was electroporated into one eye of PN0 Sprague-Dawley rats as described (Matsuda and Cepko, 2007). For the inducible expression experiments, a 2:1 ratio was used to mix with the reporter construct and ER^{T2}-Cre-ER^{T2} construct. To induce Cre-mediated recombination, a single injection of 4OH (Sigma, 2 mg/ml in corn oil**)** was subcutaneously injected into deeply anaesthetized animals (Matsuda and Cepko, 2007). Rats were housed in 12 hr light-dark cycles (6am-6pm) except for those otherwise mentioned. For constant light exposure, animals were exposed to 200 lux light intensity. Animals kept in the constant dark were housed in a temperature and humidity controlled dark cabinet (Thoren Caging Systems, PA). Tight darkness control is critically important for the observation of banding pattern of the OS proteins. All dark-adapted animals were sacrificed in the dark, and the eyes were then post-fixed in the dark. The eyes harvested from light-adapted conditions were post-fixed under room light.

Immunostaining of retinal sections and dissociated rods

Fixed retina vibratome sections were prepared and immunostained using standard free floating method (Chuang et al., 2007); detail procedures can be found in Supplemental Information. In some experiments, photoreceptors were dissociated from Sprague Dawley rats using previously described protocols (Huettner and Baughman, 1986; Pearson et al., 2012). Briefly, dissected retinas were treated with 2 unit/mL papain at 37°C for 45 min. After PBS washes, the treated retinas were fixed in 4% PFA for 10 min, washed, and triturated using fire polished Pasteur pipets. Dissociated rods were then plated on Matrigel® (2%)-coated coverslips, briefly fixed by 4% PFA, followed by immunostaining with buffers containing 0.075% saponin.

TEM, FIM-SEM and immunoEM of rodent rods

TEM morphological analyses were carried out in C57BL/6J mice or Sprague Dawley rats perfused with 4% PFA plus acrolein were processed exactly as described (Chuang et al., 2007). For FIM-SEM, C57BL/6J mice were transcardially perfused with 2.5% glutaraldehyde plus 4% PFA in 0.1 M sodium cacodylate buffer (pH 7.4). The retinal tissue blocks were counter-stained en block and embedded into EMbed-812. Samples were imaged on a FEI Helios NanoLab 650 Microscope (New York Structural Biology Center). Samples were precision milled and imaged every 10 nm at a resolution of ∼10 nm per raw pixel. Images were processed using Serial Sections Alignment Programs of IMOD/eTomo to correct drifting caused by the 30-degree angle from the block face during imaging. The images and movies presented in this paper were generated using Image J. Post-embedding immunoEM assays were carried out in CD1 mouse retinas fixed with 4% paraformaldehyde plus 0.1% glutaldehyde by transcardial perfusion.

Details of immunoEM procedures and other regents (Ab, plasmids) can be found in Supplemental Information.

Supplementary Material

Refer to Web version on PubMed Central for supplementary material.

Acknowledgments

We thank Drs. Robert Molday, Clay Smith, Jeremy Nathans, Tim MacGraw, and Connie Cepko for reagents. We also thank William Rice and Edward T. Eng. for operating and data collection of FIM-SEM at New York Structure Biology Center (supported by NYSTAR, Research facilities Improvement Program Grant number C06 RR017528-01-CEM of National Center for Research Resources, NIH, NIH grant S10 RR029300), and Dr. Jenny Xiang (Genomics Resources Core Facility, Weill Cornell Medical College) for RNA sequencing. This work was supported by Research To Prevent Blindness, the NIH (EY016805 and EY11307), and the Starr Foundation (to C.-H. S).

References

Arikawa K, Molday LL, Molday RS, Williams DS. Localization of peripherin/rds in the disk membranes of cone and rod photoreceptors: relationship to disk membrane morphogenesis and retinal degeneration. J Cell Biol. 1992; 116:659–667. [PubMed: 1730772]

Arshavsky VY. Protein translocation in photoreceptor light adaptation: a common theme in vertebrate and invertebrate vision. Sci STKE. 2003; 2003:PE43. [PubMed: 14560045]

Bascom RA, Manara S, Collins L, Molday RS, Kalnins VI, McInnes RR. Cloning of the cDNA for a novel photoreceptor membrane protein (rom-1) identifies a disk rim protein family implicated in human retinopathies. Neuron. 1992; 8:1171–1184. [PubMed: 1610568]

Battelle BA, LaVail MM. Rhodopsin content and rod outer segment length in albino rat eyes: modification by dark adaptation. Exp Eye Res. 1978; 26:487–497. [PubMed: 646863]

Baylor D. How photons start vision. Proc Natl Acad Sci U S A. 1996; 93:560–565. [PubMed: 8570595]

Bok D, Hall MO. The role of the pigment epithelium in the etiology of inherited retinal dystrophy in the rat. J Cell Biol. 1971; 49:664–682. [PubMed: 5092207]

Bolouri H, Davidson EH. Transcriptional regulatory cascades in development: initial rates, not steady state, determine network kinetics. Proc Natl Acad Sci U S A. 2003; 100:9371–9376. [PubMed: 12883007]

Chen J, Shi G, Concepcion FA, Xie G, Oprian D. Stable rhodopsin/arrestin complex leads to retinal degeneration in a transgenic mouse model of autosomal dominant retinitis pigmentosa. J Neurosci. 2006; 26:11929–11937. [PubMed: 17108167]

Chuang JZ, Vega C, Jun W, Sung CH. Structural and functional impairment of endocytic pathways by retinitis pigmentosa mutant rhodopsin-arrestin complexes. J Clin Invest. 2004; 114:131–140. [PubMed: 15232620]

Chuang JZ, Zhao Y, Sung CH. SARA-regulated vesicular targeting underlies formation of the light-sensing organelle in mammalian rods. Cell. 2007; 130:535–547. [PubMed: 17693260]

Cohen AI. The ultrastructure of the rods of the mouse retina. Am J Anatom. 1960; 107:23–48.

Cohen AI. Some cytological and initial biochemical observations on photoreceptors in retinas of rds mice. Invest Ophthalmol Vis Sci. 1983; 24:832–843. [PubMed: 6862791]

Corless JM, Kaplan MW. Structural interpretation of the birefringence gradient in retinal rod outer segments. Biophys J. 1979; 26:543–556. [PubMed: 262431]

De Robertis E. Some observations on the ultrastructure and morphogenesis of photoreceptors. J Gen Physiol. 1960; 43:1–13. [PubMed: 13814989]

Fekete DM, Barnstable CJ. The subcellular localization of rat photoreceptor-specific antigens. J Neurocytol. 1983; 12:785–803. [PubMed: 6358424]

Goldberg AFX, Molday RS. Subunit composition of the peripherins/rds-Rom-1 disk rim complex from rod photoreceptors: hydrodynamic evidence for a tetrameric quaternary structure. Biochemistry. 1996; 35:6144–6149. [PubMed: 8634257]

Gurevich VV, Hanson SM, Song X, Vishnivetskiy SA, Gurevich EV. The functional cycle of visual arrestins in photoreceptor cells. Prog Retin Eye Res. 2011; 30:405–430. [PubMed: 21824527]

Haeri M, Calvert PD, Solessio E, Pugh EN Jr, Knox BE. Regulation of Rhodopsin-eGFP Distribution in Transgenic Xenopus Rod Outer Segments by Light. PLoS One. 2013; 8:e80059. [PubMed: 24260336]

Hartong DT, Berson EL, Dryja TP. Retinitis pigmentosa. Lancet. 2006; 368:1795–1809. [PubMed: 17113430]

Hawkins RK, Jansen HG, Sanyal S. Development and degeneration of retina in rds mutant mice: photoreceptor abnormalities in the heterozygotes. Exp Eye Res. 1985; 41:701–720. [PubMed: 3830736]

Hicks D, Molday RS. Differential immunogold-dextran labeling of bovine and frog rod and cone cells using monoclonal antibodies against bovine rhodopsin. Exp Eye Res. 1986; 42:55–71. [PubMed: 2420630]

Huettner JE, Baughman RW. Primary culture of identified neurons from the visual cortex of postnatal rats. J Neurosci. 1986; 6:3044–3060. [PubMed: 3760948]

Humphries M, rancourt D, farrar G, Kenna P, Hazel M, Bush R, Sieving P, Sheils D, McNally N, Creighton P, et al. Retinopathy induced in mice by targated disruption of the rhodopsin gene. Nat Genetics. 1997; 15:216–219. [PubMed: 9020854]

Insinna C, Besharse JC. Intraflagellar transport and the sensory outer segment of vertebrate photoreceptors. Dev Dyn. 2008; 237:1982–1992. [PubMed: 18489002]

Jan LY, Revel JP. Ultrastructural localization of rhodospin in the vertebrate retina. J Cell Biol. 1974; 62:257–273. [PubMed: 4139160]

Jin S, Cornwall MC, Oprian DD. Opsin activation as a cause of congenital night blindness. Nature neuroscience. 2003; 6:731–735.

Kaplan MW. Light cycle--dependent axial variations in frog rod outer segment structure. Invest Ophthalmol Vis Sci. 1981; 21:395–402. [PubMed: 6974155]

Kedzierski W, Moghrabi WN, Allen AC, Jablonski-Stiemke MM, Azarian SM, Bok D, Travis GH. Three homologs of rds/peripherin in Xenopus laevis photoreceptors that exhibit covalent and non-covalent interactions. J Cell Sci. 1996; 109(Pt 10):2551–2560. [PubMed: 8923216]

LaVail MM. Kinetics of rod outer segment renewal in the developing mouse retina. J Cell Biol. 1973; 58:650–661. [PubMed: 4747920]

LaVail MM. Outer segment disc shedding and phagocytosis in the outer retina. Trans Ophthalmol Soc U K. 1983; 103:397–404. [PubMed: 6380008]

Lem J, Krasnoperova NV, Calvert PD, Kosaras B, Cameron DA, Nicolo M, Makino CL, Sidman RL. Morphological, physiological, and biochemical changes in rhodopsin knockout mice. Proc Natl Acad Sci U S A. 1999; 96:736–741. [PubMed: 9892703]

Loewen CJ, Moritz OL, Tam BM, Papermaster DS, Molday RS. The role of subunit assembly in peripherin-2 targeting to rod photoreceptor disk membranes and retinitis pigmentosa. Mol Biol Cell. 2003; 14:3400–3413. [PubMed: 12925772]

MacKenzie D, Arendt A, Hargrave P, McDowell JH, Molday RS. Localization of binding sites for carboxyl terminal specific anti-rhodopsin monoclonal antibodies using synthetic peptides. Biochemistry. 1984; 23:6544–6549. [PubMed: 6529569]

Matsuda T, Cepko CL. Controlled expression of transgenes introduced by in vivo electroporation. Proc Natl Acad Sci U S A. 2007; 104:1027–1032. [PubMed: 17209010]

Moaven H, Koike Y, Jao CC, Gurevich VV, Langen R, Chen J. Visual arrestin interaction with clathrin adaptor AP-2 regulates photoreceptor survival in the vertebrate retina. Proc Natl Acad Sci U S A. 2013; 110:9463–9468. [PubMed: 23690606]

Molday RS, Hicks D, Molday L. Peripherin. A rim-specific membrane protein of rod outer segment discs. Invest Ophthalmol Vis Sci. 1987; 28:50–61. [PubMed: 2433249]

Nir I, Papermaster DS. Differential distribution of opsin in the plasma membrane of frog photoreceptor. An immunocytochemical study. Invest Ophthalmol Vis Sci. 1983; 24:868–878. [PubMed: 6223003]

Organisciak DT, Noell WK. The rod outer segment phospholipid/opsin ratio of rats maintained in darkness or cyclic light. Invest Ophthalmol Vis Sci. 1977; 16:188–190. [PubMed: 832982]

Papermaster DS, Schneider BG, Zorn MA, Kraehenbuhl JP. Immunocytochemical localization of a large intrinsic membrane protein to the incisures and margins of frog rod outer segment disks. The Journal of cell biology. 1978; 78:415–425. [PubMed: 690173]

Pearson RA, Barber AC, Rizzi M, Hippert C, Xue T, West EL, Duran Y, Smith AJ, Chuang JZ, Azam SA, et al. Restoration of vision after transplantation of photoreceptors. Nature. 2012; 485:99–103. [PubMed: 22522934]

Pedler CM, Tilly R. The fine structure of photoreceptor discs. Vision Res. 1967; 7:829–836. [PubMed: 4182125]

Penn JS, Anderson RE. Effect of light history on rod outer-segment membrane composition in the rat. Exp Eye Res. 1987; 44:767–778. [PubMed: 3653272]

Penn JS, Williams TP. Photostasis: regulation of daily photon-catch by rat retinas in response to various cyclic illuminances. Exp Eye Res. 1986; 43:915–928. [PubMed: 3817032]

Poetsch A, Molday LL, Molday RS. The cGMP-gated channel and related glutamic acid-rich proteins interact with peripherin-2 at the rim region of rod photoreceptor disc membranes. J Biol Chem. 2001; 276:48009–48016. [PubMed: 11641407]

Raman D, Osawa S, Gurevich VV, Weiss ER. The interaction with the cytoplasmic loops of rhodopsin plays a crucial role in arrestin activation and binding. J Neurochem. 2003; 84:1040–1050. [PubMed: 12603828]

Rattner A, Smallwood PM, Williams J, Cooke C, Savchenko A, Lyubarsky A, Pugh EN, Nathans J. A photoreceptor-specific cadherin is essential for the structural integrity of the outer segment and for photoreceptor survival. Neuron. 2001; 32:775–786. [PubMed: 11738025]

Ritter LM, Boesze-Battaglia K, Tam BM, Moritz OL, Khattree N, Chen SC, Goldberg AF. Uncoupling of photoreceptor peripherin/rds fusogenic activity from biosynthesis, subunit assembly, and targeting: a potential mechanism for pathogenic effects. J Biol Chem. 2004; 279:39958–39967. [PubMed: 15252042]

Robinson PR, Cohen GB, Zhukovsky EA, Oprian DD. Constitutively active mutants of rhodopsin. Neuron. 1992; 9:719–725. [PubMed: 1356370]

Rohlich P. The sensory cilium of retinal rods is analogous to the transitional zone of motile cilia. Cell Tissue Res. 1975; 161:421–430. [PubMed: 1175211]

Sanyal S, Jansen HG. Absence of receptor segments in the retina of rds mutant mice. Neurosci Lett. 1981; 21:23–26. [PubMed: 7207866]

Shi W, Sports CD, Raman D, Shirakawa S, Osawa S, Weiss ER. Rhodopsin arginine-135 mutants are phosphorylated by rhodopsin kinase and bind arrestin in the absence of 11-cis-retinal. Biochemistry. 1998; 37:4869–4874. [PubMed: 9538004]

Sung CH, Makino C, Baylor D, Nathans J. A rhodopsin gene mutation responsible for autosomal dominant retinitis pigmentosa results in a protein that is defective in localization to the photoreceptor outer segment. J Neuro. 1994; 14:5818–5833.

Sung CH, Chuang JZ. The cell biology of vision. J Cell Biol. 2010; 190:953–963. [PubMed: 20855501]

Tam BM, Moritz OL, Hurd LB, Papermaster DS. Identification of an outer segment targeting signal in the COOH terminus of rhodopsin using transgenic Xenopus laevis. J Cell Biol. 2000; 151:1369–1380. [PubMed: 11134067]

Tam BM, Moritz OL, Papermaster DS. The C terminus of peripherin/rds participates in rod outer segment targeting and alignment of disk incisures. Mol Biol Cell. 2004; 15:2027–2037. [PubMed: 14767063]

Thuenauer R, Hsu YC, Carvajal-Gonzalez JM, Deborde S, Chuang JZ, Romer W, Sonnleitner A, Rodriguez-Boulan E, Sung CH. Four-dimensional live imaging of apical biosynthetic trafficking reveals a post-Golgi sorting role of apical endosomal intermediates. Proc Natl Acad Sci U S A. 2014; 111:4127–4132. [PubMed: 24591614]

Travis GH, Brennan MB, Danielson PE, Kozak CA, Sutcliffe JG. Identification of a photoreceptor-specific mRNA encoded by the gene responsible for retinal degeneration slow (rds). Nature. 1989; 338:70–73. [PubMed: 2918924]

Travis GH, Sutcliffe JG, Bok D. The retinal degeneration slow (*rds*) gene product is a photoreceptor disc membrane-associated glycoprotein. Neuron. 1991; 6:61–70. [PubMed: 1986774]

Weisz OA, Rodriguez-Boulan E. Apical trafficking in epithelial cells: signals, clusters and motors. J Cell Sci. 2009; 122:4253–4266. [PubMed: 19923269]

Wen XH, Shen L, Brush RS, Michaud N, Al-Ubaidi MR, Gurevich VV, Hamm HE, Lem J, Dibenedetto E, Anderson RE, et al. Overexpression of rhodopsin alters the structure and photoresponse of rod photoreceptors. Biophys J. 2009; 96:939–950. [PubMed: 19186132]

Whelan JP, McGinnis JF. Light-dependent subcellular movement of photoreceptor proteins. J Neurosci Res. 1988; 20:263–270. [PubMed: 3172281]

Williams TP, Squitieri A, Henderson RP, Webbers JP. Reciprocity between light intensity and rhodopsin concentration across the rat retina. J Physiol. 1999; 516(Pt 3):869–874. [PubMed: 10200432]

Wrigley JD, Ahmed T, Nevett CL, Findlay JB. Peripherin/rds influences membrane vesicle morphology. Implications for retinopathies. J Biol Chem. 2000; 275:13191–13194. [PubMed: 10747861]

Yeh TY, Peretti D, Chuang JZ, Rodriguez-Boulan E, Sung CH. Regulatory dissociation of Tctex-1 light chain from dynein complex is essential for the apical delivery of rhodopsin. Traffic. 2006; 7:1495–1502. [PubMed: 16956385]

Young RW. The renewal of photoreceptor cell outer segments. J Cell Biol. 1967; 33:61–72. [PubMed: 6033942]

Young RW. Passage of newly formed protein through the connecting cilium of retinal rods in the frog. J Ultrastruct Res. 1968; 23:462–473. [PubMed: 5692302]

Young RW. Shedding of discs from rod outer segments in the rhesus monkey. J Ultrastruct Res. 1971; 34:190–203. [PubMed: 4992906]

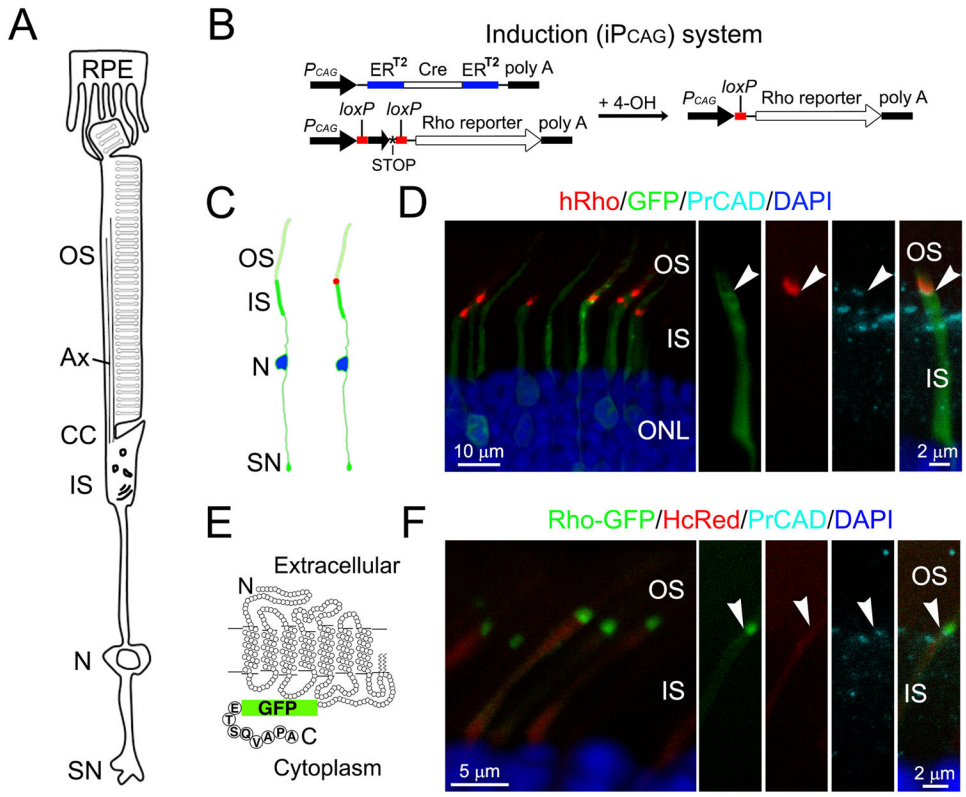

Figure 1. Inducible expression of rhodopsin reporters in mature rods

(**A**) A schematic drawing depicting the compartmentalized structure of a mammalian rod and its interaction with RPE cells. Ax: axoneme; CC: connecting cilium; N: nucleus, SN: synapse. (**B**) A diagram depicting the Cre-loxP based method to induce the expression of the rhodopsin reporter (i.e., iP_{CAG} system). ER^{T2}-Cre-ER^{T2} is co-transfected with the rhodopsin reporter gene that is downstream of a loxP-neo-STOP-loxP cassette. Addition of 4OH activates the Cre activity, removes the loxP cassette, and activates the reporter gene expression. (**C**) A cartoon illustrating a predicted expression pattern of co-transfected P_{CAG}-IRES-GFP and iP_{CAG}-hRho before (left) and 1-day after (right) 4OH induction. (**D**) Rods transfected with P_{CAG}-IRES-GFP and iP_{CAG}-hRho harvested from a rat 24-hr post 4OH induction and 1-hr dark adaptation. PrCAD: photoreceptor-cadherin. (**E**) A drawing of the coding sequence of the Rho-GFP construct. Other fluorescent rhodopsin reporters were created using the same strategy. (**F**) Rods transfected with P_{CAG}-HcRed and iP_{CAG}-Rho-GFP harvested from a rat 24-hr post 4OH induction and 1-hr dark adaptation. Arrowheads point to the junctions between the IS and the OS. ONL: outer nuclear layer. See also Figure S1.

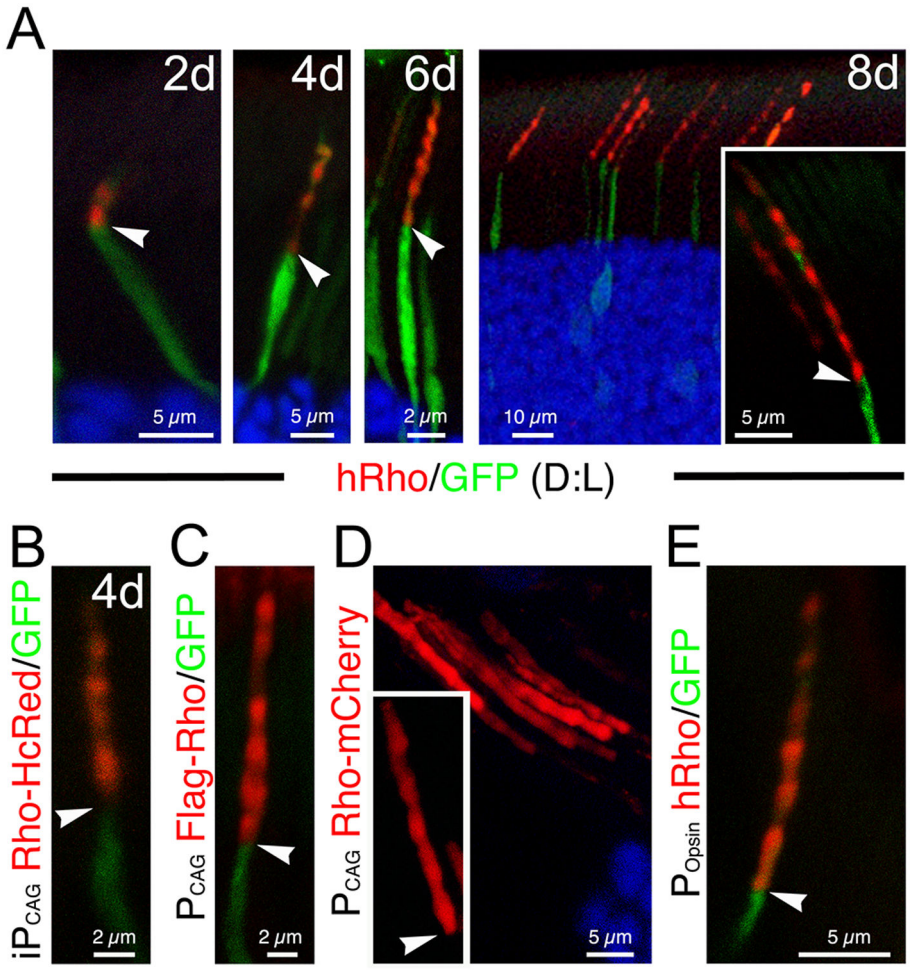

Figure 2. The OS entry of rhodopsin follows a diurnal rhythm

(**A**) Representative 3A6 mAb immunolabeling (red) of rods transfected with iP_{CAG}-hRho and P_{CAG}-GFP. All rats were reared under the usual 12 hr:12 hr dark: light (D:L) for the indicated number of days. (**B**) An example of representative rods transfected iP_{CAG}-Rho-HcRed and P_{CAG}-IRES-GFP 4 days after 4OH induction. (**C**) Flag immunolabeling (red) of a representative rod transfected with P_{CAG}-FLAG-Rho-IRES-GFP. (**D**) Direct fluorescence visualization of rods transfected with P_{CAG}-Rho-mCherry. (**E**) 3A6 mAb immunolabeling (red) of a representative rod constitutively expressing hRho-IRES-GFP under the P_{opsin} promoter. All arrowheads point to the IS-OS junctions. See also Figure S2.

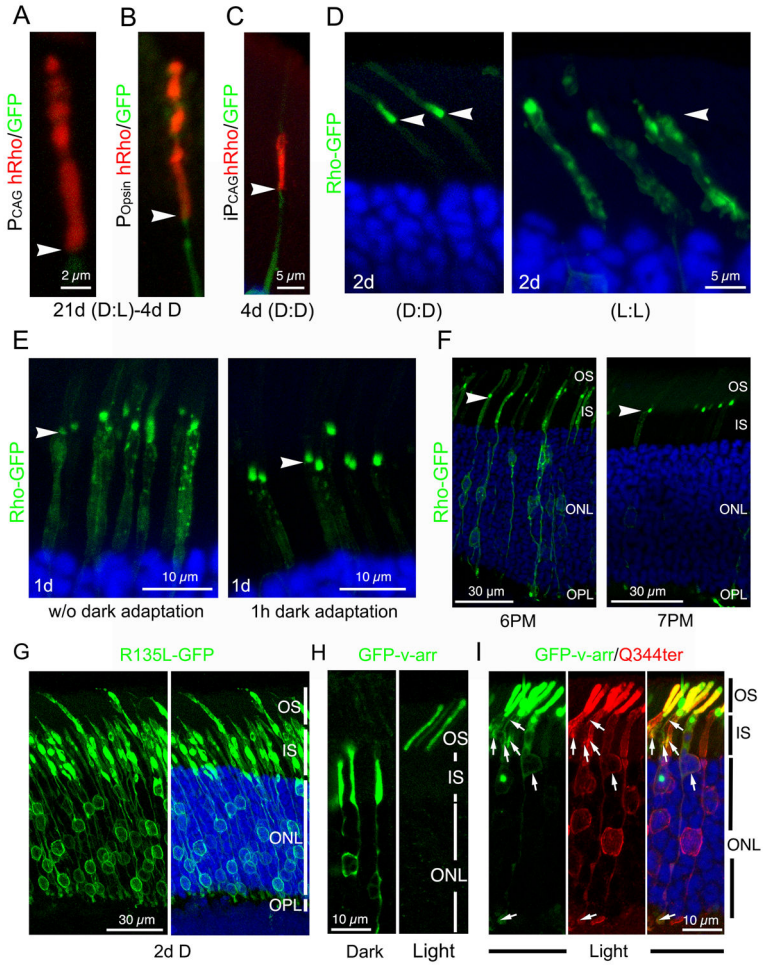

Figure 3. Light inhibits the OS entry of rhodopsin

(**A, B**) hRho immunolabeling (red) of a rod expressing P_{CAG}-hRho-IRES-GFP (A) or P_{Opsin}-hRho-IRES-GFP (B) in rats reared in the usual dark-light cycle and then switched to complete darkness for 4 days prior to harvest. (**C**) hRho immunolabeling (red) of a rod co-transfected with P_{CAG}-IRES-GFP and iP_{CAG}-hRho of rats kept in darkness during the 4-day 4OH induction. (**D**) Rods induced to express iP_{CAG}-Rho-GFP for 2 days in constant dark (D;D) or constant ambient light (L:L). (**E**) One day after 4OH induction, rods transfected with iP_{CAG}-Rho-GFP were harvested at noon after a 1-hr dark adaptation (right panel) or without the dark adaptation (left panel). (**F**) Rods transfected with iP_{CAG}-Rho-GFP were induced to express for ∼48 hr and then harvested at either 6 PM or 7 PM. Arrowheads in (A-F) point to the IS-OS junctions. (**G**) Rods transfected with iP_{CAG}-R135L-GFP were kept in dark for 2 days after 4OH induction. (**H**) Rods transfected with P_{CAG}-GFP-v-arr were harvested under dark or light conditions. (**I**) Q344ter immunolabeling (red) of rods transfected with P_{CAG}-Q344ter-IRES-GFP-v-arr and harvested in light. Arrows point to the co-localized GFP-v-arr and Q344ter rhodopsin in the IS/cell bodies/synapses. See also Figure S3.

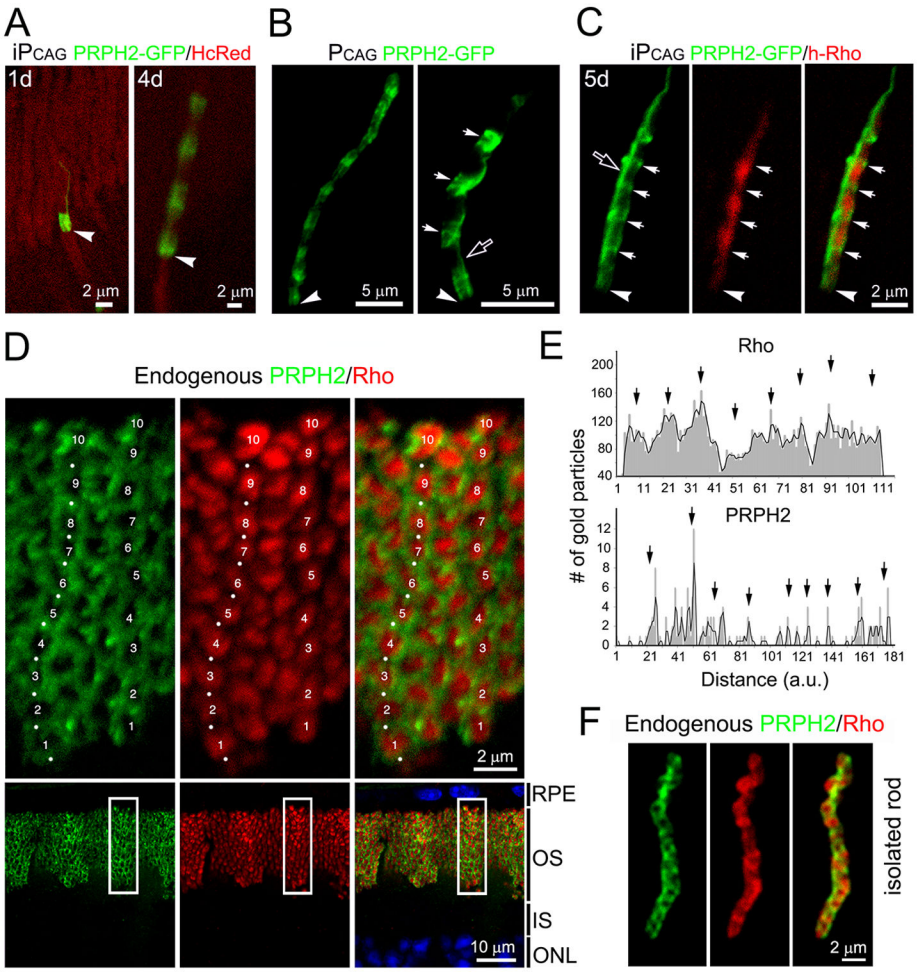

Figure 4. OS discs enriched with rhodopsin and PRPH2 are alternately arrayed

(**A**) Representative rods co-transfected with iP_{CAG}-PRPH2-GFP and P_{CAG}-HcRed harvested 1 day or 4 days post 4OH induction. (**B**) Left: a rod constitutively expressing PRPH2-GFP. Right: a highly magnified view of PRPH2-GFP+ bands, which had a more irregular shape (arrows). (**C**) 3A6 mAb immunolabeling of a rod co-transfected with iP_{CAG}- PRPH2-GFP and iP_{CAG}-hRho for 5 days. Arrows point to the bands containing strong PRPH2-GFP but weak hRho signals. Arrowheads in (A-C) point to the IS-OS junctions; open arrows in (B, C) show the PRPH2-GFP+ signals longitudinally aligned with the OS axoneme. (**D**) C57BL6/J mouse retinal slice pretreated with neuraminidase and labeled for endogenous PRPH2 (green, white dots) and rhodopsin (red) using 5H2 mAb and C107 rabbit Abs, respectively. Top panels show the enlarged views of the boxed areas in the bottom panels. Numbers 1 to 10 mark the 10 distinguishable segments containing a higher level of rhodopsin and a lower level of PRPH2 in two rod OS. (**E**) The numbers of immunogolds that labeled endogenous rhodopsin and PRPH2 were plotted against the distance from the basalmost (zero) to the distalmost OS in arbitrary units (a.u.); black arrows point to the peak signals. Representative results of one rod for each molecule (out of total 6 rods examined) are shown. (**F**) Representative image of a dissociated rod co-labeled for endogenous PRPH2 (green) and rhodopsin (red). See also Figure S4 and Movie 1.

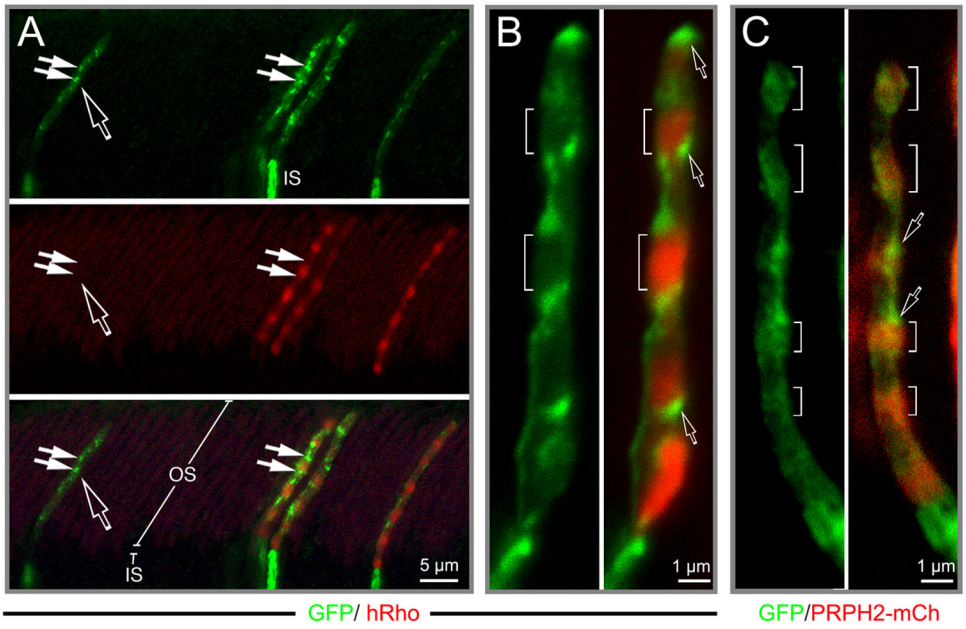

Fig. 5. Spatial organization of the OS cytoplasmic spaces

(**A**) Rats with rods co-transfected with P_{CAG}-GFP and P_{CAG}-hRho were reared in regular cyclic light until harvest. A low-power confocal image showing a GFP (green) and 3A6 (red) Ab-labeled retinal slice containing four transfected rods; open arrow points to a rod singly transfected with GFP and another three rods expressing both hRho and GFP. (**B**) An example of representative rod OS that co-expressed GFP (green) and hRho (red). Brackets mark the Rho-rich segments that had weak GFP signal; open arrows point to the hotspots expressing highest GFP signal. (**C**) A representative rod OS that co-expressed GFP and PRPH2-mCherry. Brackets mark the PRPH2-rich segments (red) that had modest GFP signal; open arrows point to the GFP hotspots. See also Figures S5 and S6 and Movies 2, 3.

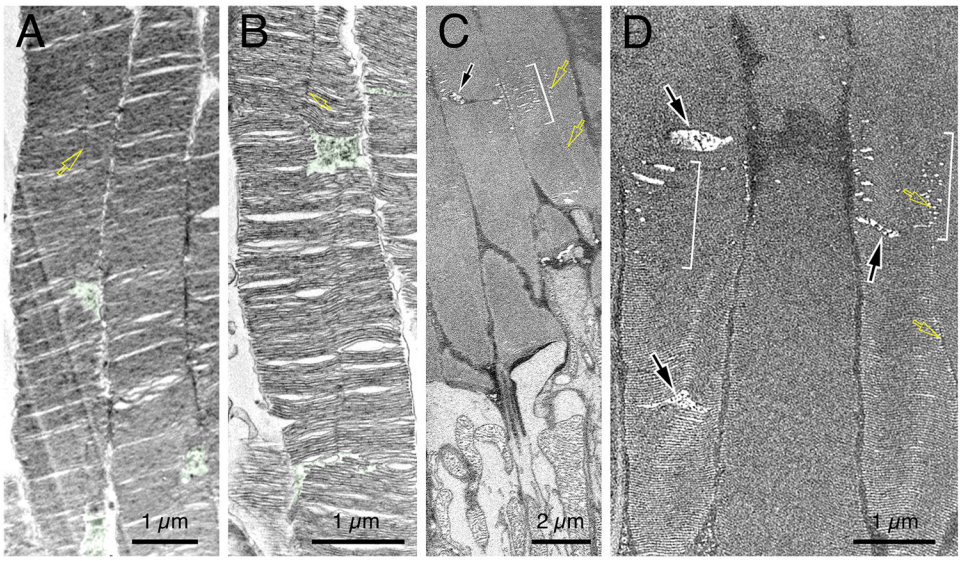

Fig. 6. Ultrastructural analysis of the OS heterogeneity and OSCPs

(**A, B**) TEM examination of the longitudinal sectioning views of the proximal-to-middle section of mouse rod OS. The characteristic OSCPs were highlighted in green. The vertical lines running along the OS axis represent the incisures that aligned along the stacked discs (yellow arrows). (**C**, **D**) Two representative block-face images of mouse rod OS examined by FIM-SEM. Brackets mark discs had obviously porous appearance. Black arrows point to the characteristic OSCP. Yellow arrows point to incisures. (**C**) is a still image representing a partial area of Movie 4. See also Figures S5 and S6.

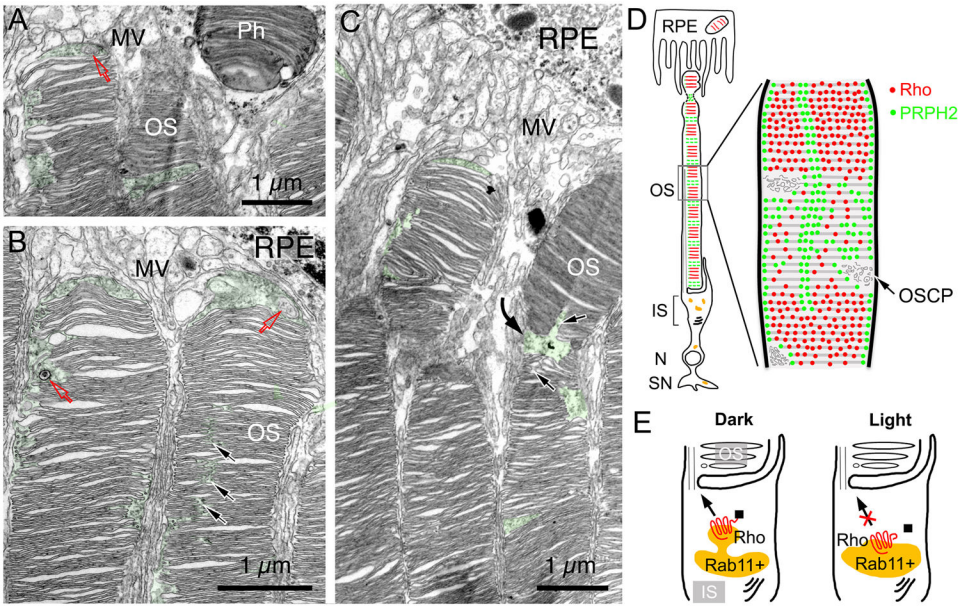

Fig. 7. Distal OS organization and working models

(**A-C**) Three representative TEM images of the distal region of rat rod OS. Characteristic OPSC were highlighted in green. Red arrows point to the MVB/autophagosome-like structures inside the OSCP and the OS apex cytoplasmic space. Black arrows in (B) point to the less spatially confined OSCP; black arrows in (C) point to the areas where the discs have enlarged incisures. The curved arrow in (C) points to the bent OS tip. Sd: shedde discs; MV: microvilli. (**D**) Cartoons delineate the organization of heterogeneous discs and OSCP. Rod OS discs are organized into ∼10 main fractions, each containing the discs synthesized in one day. The discs enriched with rhodopsin (red) are alternated with the discs enriched with PRPH2 (green). Discs expressing a higher level of PRPH2 are likely to exhibit larger rims/incisures. This may explain their enlarged cytoplasmic contacts and a more fragmented (porous) appearance. We hypothesized that PRPH2-rich discs are more susceptible to structural changes, possibly serving as pre-marked breaking points during disc shedding at the distal tip. Note that PRPH2 (green) is also expressed on the rims and the incisures of all discs. OSCP are situated at the transition between rhodopsin- and PRPH2-rich disc stacks. (**E**) Our data suggest that the exit of newly synthesized rhodopsin from the post-Golgi, intermediate compartment of IS (e.g., $Rab11^{+}$ endosome) is highly regulated; dark provides a permissive signal, whereas light provides an inhibitory signal. We hypothesized that the regulation may be related to rhodopsin's light-mediated conformational change and the resulting ability to bind the OS transport machinery (■).